*Inorg. Chem.* **2006**, *45*, 8729–8735


# Theoretical Insight into Electronic Structures and Spectroscopic Properties of $[Pt_2(pop)_4]^{4-}$, $[Pt_2(pcp)_4]^{4-}$, and Related Derivatives (pop = $P_2O_5H_2^{2-}$ and pcp = $P_2O_4CH_4^{2-}$)

**Qing-Jiang Pan,[†] Hong-Gang Fu,*[,†] Hai-Tao Yu,[†] and Hong-Xing Zhang[‡]**

*School of Chemistry and Materials Science, Heilongjiang University, Harbin 150080, China, and State Key Laboratory of Theoretical and Computational Chemistry, Institute of Theoretical Chemistry, Jilin University, Changchun 130023, China*

Received February 28, 2006

The structures of $[Pt_2(pop)_4]^{4-}$, $[Pt_2(pcp)_4]^{4-}$, and related species $[Pt_2(pop)_4X_2]^{4-}$ and $[Pt_2(pop)_4]^{2-}$ in the ground states (pop = $P_2O_5H_2^{2-}$, pcp = $P_2O_4CH_4^{2-}$, and X = I, Br, and Cl) were optimized using the second-order Møller–Plesset perturbation (MP2) method. It is shown that the Pt–Pt distances decrease in going from $[Pt_2(pop)_4]^{4-}$ to $[Pt_2(pop)_4X_2]^{4-}$ to $[Pt_2(pop)_4]^{2-}$. This is supported by the analyses of their electronic structures. The calculated aqueous absorption spectra at the time-dependent density functional theory (TD-DFT) level agree with experimental observations. The unrestricted MP2 method was employed to optimize the structures of $[Pt_2(pop)_4]^{4-}$ and $[Pt_2(pcp)_4]^{4-}$ in the lowest-energy triplet excited states. The Pt–Pt contraction trend is well reproduced in these calculations. For $[Pt_2(pop)_4]^{4-}$, the Pt–Pt distance decreases from 2.905 Å in the ground state to 2.747 Å in the excited state, which is comparable to experimental values of 2.91–2.92 Å and 2.64–2.71 Å, respectively. On the basis of the excited-state structures of such complexes, TD-DFT predicts the solution emissions at 480 and 496 nm, which is closer to the experimental values of 512 and 510 nm emissions, respectively.

## Introduction

Since the discovery[1,2] of the famous complex $[Pt_2(pop)_4]^{4-}$ (pop = $P_2O_5H_2^{2-}$), great interest in its properties has developed.[3−10] It is now well established by spectroscopic experiments that $[Pt_2(pop)_4]^{4-}$ exhibits an intense green phosphorescence in solution at room temperature because of a $\sigma(p) \rightarrow \sigma^*(d)$ transition.[3,4] Because of its long lifetime (9.5 $\mu$s) and high quantum yield (>0.5), the triplet excited state, $[Pt_2(pop)_4]^{4-*}$, possesses unusual photochemical properties.[5−8] It reacts with added quenchers by mechanisms that involve the platinum complex as an oxidant, reductant, or atom-transfer reagent.[5−7] For example, the highly reactive $[Pt_2(pop)_4]^{4-*}$ can abstract hydrogen atoms from a wide range of substrates including alcohols, hydrocarbons, silanes, and stannanes, as well as halogen atoms from alkyl and aryl halides.[7]

Furthermore, when $[Pt_2(pop)_4]^{4-}$ is treated with halogen, binuclear dihaloplatinum(III) $[Pt_2(pop)_4X_2]^{4-}$ complexes are formed by oxidative addition.[11−14] These complexes retain

* To whom correspondence should be addressed. E-mail: fuhg@vip.sina.com.
† Heilongjiang University.
‡ Jilin University.

(1) Sperline, R. P.; Dickson, M. K.; Roundhill, D. M. *J. Chem. Soc., Chem. Commun.* **1977**, 62.
(2) Filomena dos Remedios Pinto, M. A.; Sadler, P. J.; Neidle, S.; Sanderson, M. R.; Subbiah, A.; Kuroda, R. *J. Chem. Soc., Chem. Commun.* **1980**, 13.
(3) Fordyce, W. A.; Brummer, J. G.; Grosby, G. A. *J. Am. Chem. Soc.* **1981**, *103*, 7061.
(4) (a) Che, C.-M.; Butler, L. G.; Gray, H. B. *J. Am. Chem. Soc.* **1981**, *103*, 7796. (b) Rice, S. F.; Gray, H. B. *J. Am. Chem. Soc.* **1983**, *105*, 4571. (c) Roundhill, D. M.; Gray, H. B.; Che, C.-M. *Acc. Chem. Res.* **1989**, *22*, 55.
(5) (a) Heuer, W. B.; Totten, M. D.; Rodman, G. S.; Hebert, E. J.; Tracy, H. J.; Nagle, J. K. *J. Am. Chem. Soc.* **1984**, *106*, 1163. (b) Peterson, J. R.; Kalyanasundaram, K. *J. Phys. Chem.* **1985**, *89*, 2486. (c) Herman, M. S.; Goodman, J. L. *Inorg. Chem.* **1991**, *30*, 1147.
(6) (a) Roundhill, D. M. *J. Am. Chem. Soc.* **1985**, *107*, 4354. (b) Roundhill, D. M.; Atherton, S. J. *Inorg. Chem.* **1986**, *25*, 4071. (c) Roundhill, D. M.; Shen, Z.-P.; Atherton, S. J. *Inorg. Chem.* **1987**, *26*, 3833.
(7) (a) Vlèek, A., Jr.; Gray, H. B. *Inorg. Chem.* **1987**, *26*, 1997. (b) Harvey, E. L.; Stiegman, A. E.; Vlèek, A., Jr.; Gray, H. B. *J. Am. Chem. Soc.* **1987**, *109*, 5233. (c) Che, C.-M.; Lee, W.-M.; Cho, K.-C.; Harvey, P. D.; Gray, H. B. *J. Phys. Chem.* **1989**, *93*, 3095. (d) Sweeney, R. J.; Harvey, E. L.; Gray, H. B. *Coord. Chem. Rev.* **1990**, *105*, 23.
(8) (a) Kalsbeck, W. A.; Grover, N.; Thorp, H. H. *Angew. Chem., Int. Ed. Engl.* **1991**, *30*, 1517. (b) Kalsbeck, W. A.; Gingell, D. M.; Malinsky, J. E.; Thorp, H. H. *Inorg. Chem.* **1994**, *33*, 3313. (c) Ciftan, S. A.; Thorp, H. H. *J. Am. Chem. Soc.* **1998**, *120*, 9995.
(9) Dickson, M. K.; Pettee. S. K.; Roundhill, D. M. *Anal. Chem.* **1981**, *53*, 2159.
(10) Roundhill, D. M. *Sol. Energy* **1986**, *36*, 297.

10.1021/ic060336v CCC: $33.50 
Published on Web 09/20/2006

the basic skeleton of $[Pt_2(pop)_4]^{4-}$ but also contain axial Pt−X bonds and a Pt−Pt single bond. The Pt−Pt distances in $K_4[Pt_2(pop)_4X_2]$ (X = I, Br, and Cl)[11−13] range from 2.75 to 2.69 Å, which is considerably shorter than a distance of 2.92 Å in $K_4[Pt_2(pop)_4]\cdot 2H_2O$.[2] In view of a simple molecular orbital (MO) theory,[15] the binuclear $d^8$ complex $[Pt_2(pop)_4]^{4-}$ with $(d\sigma)^2(d\sigma^*)^2$ configuration has a formal bond order of zero, while a single bond is given to the binuclear $d^7$ complexes $[Pt_2(pop)_4X_2]^{4-}$ with a filled $(d\sigma)^2$ orbital. The lower energy bands in the absorption spectra of the $[Pt_2(pop)_4X_2]^{4-}$ complexes have been ascribed to excitations to the empty $d\sigma^*$ orbital.[11ac,14] The oxidative reactions have led to a loss of luminescence of the halide complexes.

A structurally analogous complex is $[Pt_2(pcp)_4]^{4-}$ (pcp = $P_2O_4CH_4^{2-}$), which differs from $[Pt_2(pop)_4]^{4-}$ by having a methylenic group rather than an oxygen atom in the ligand bridge.[16] The electronic spectroscopy of the two complexes (both absorption and emission) is very similar. The only major difference is that the triplet lifetime of $[Pt_2(pcp)_4]^{4-*}$ in aqueous solution at ambient temperature under anaerobic conditions is 55 ns, whereas that of $[Pt_2(pop)_4]^{4-*}$ is 9.5 $\mu$s. Transient difference spectroscopy experiments showed that the former is more reactive than the latter in the reactions with alkyl and aryl halide, hydrogen atom donors, etc.[16b]

As suggested in the literature,[3−7] the metal-localized $\sigma^*(d) \rightarrow \sigma(p)$ transition of $[Pt_2(pop)_4]^{4-}$ leads to a contracted Pt−Pt distance in the excited state relative to one in the ground state. Recently, Coppens[17a] and Rillema[17b] used density functional theory (DFT) methods to study the electronic properties of $[Pt_2(pop)_4]^{4-}$. The calculated Pt−Pt distances are 3.04 and 2.82 Å in the ground state and triplet excited state, respectively, compared with 2.92 and 2.64−2.71 Å distances determined by experiments.[2,3,4b,18−21] Although there have been some studies on the electronic structures of $[Pt_2(pop)_4]^{4-}$,[17] few theoretical investigations on the spectroscopic properties of $[Pt_2(pcp)_4]^{4-}$ and $[Pt_2(pop)_4X_2]^{4-}$ (X = I, Br and Cl) have been done.

To provide a clear picture of binuclear $d^8$ complexes in the electronic structures and to gain an insight into their spectroscopic properties, we employed theoretical methods to explore the ground- and excited-state properties of $[Pt_2(pop)_4]^{4-}$, $[Pt_2(pcp)_4]^{4-}$, $[Pt_2(pop)_4X_2]^{4-}$ (X = I, Br, and Cl), and $[Pt_2(pop)_4]^{2-}$. The six complexes in sequence are labeled as **pop**, **pcp**, **popI**, **popBr**, **popCl**, and **pop**$^{2+}$. The second-order Møller−Plesset perturbation (MP2)[22] and unrestricted MP2 (UMP2) calculations on **pop** and **pcp** show that upon excitation the Pt−Pt distances shorten 0.158 and 0.174 Å with respect to the 2.905 and 2.987 Å distances in the ground states, respectively. The $\sigma^*(d_{z^2}) \rightarrow \sigma(p_z)$ transition makes the Pt−Pt interaction in the excited state close to a $\sigma$ single bond. On the basis of the time-dependent density functional theory (TD-DFT)[23] calculations, we simulated the absorption spectrum in water. This is well correlated with the experimental absorption spectrum.

## Computational Details

We used the MP2 method to optimize the structures of **pop**, **pcp**, **popI**, **popBr**, **popCl**, and **pop**$^{2+}$ in the ground states. The optimizations on the first two complexes in the lowest-energy triplet excited states were performed at UMP2 levels. It has been well established that the transition energies calculated by the TD-DFT method are comparable in accuracy to those by the higher-level configuration interaction methods.[24] On the basis of the ground- and excited-state structures of complexes, we employed the TD-DFT (Becke's 3 parameter hybrid functional using the Lee−Yang−Parr correlation functional, B3LYP)[25] method to predict the absorption and emission spectra. We performed calculations using Hay and Wadt[26] effective core potentials (ECPs) for Pt, I, Br, Cl, and P. The LanL2DZ basis sets associated with the ECPs were employed. To describe the Pt−Pt interaction and the molecular properties precisely, one additional function was implemented for Pt ($\alpha_f = 0.18$), I ($\alpha_d = 0.266$), Br ($\alpha_d = 0.389$), Cl ($\alpha_d = 0.514$), and P ($\alpha_d = 0.34$).[27]

The calculation on the single molecule model corresponds to the behaviors of the complex in the gas phase. We considered the influence of solvent molecules on spectroscopic properties of complexes that was indicated in the previous work,[17b,28] and then we employed the polarized continuum model (PCM) in the self-


(11) (a) Che, C.-M.; Schaefer, W. P.; Gray, H. B.; Dickson, M. K.; Stein, P. B.; Roundhill, D. M. *J. Am. Chem. Soc.* **1982**, *104*, 4253. (b) Che, C.-M.; Herbstein, F. H.; Schaefer, W. P.; Marsh, R. E.; Gray, H. B. *J. Am. Chem. Soc.* **1983**, *105*, 4604. (c) Che, C.-M.; Butler, L. G.; Brunthaner, P. J.; Gray, H. B. *Inorg. Chem.* **1985**, *24*, 4662.

(12) (a) Alexander, K. A.; Bryan, S. A.; Fronczek, F. R.; Fultz, W. C.; Rheingold, A. L.; Roundhill, D. M.; Stein, P.; Watkins, S. F. *Inorg. Chem.* **1985**, *24*, 2803. (b) Clark, R. J. H.; Kurmoo, M.; Dawes, H. M.; Hursthouse, M. B. *Inorg. Chem.* **1986**, *25*, 409.

(13) Zipp, A. P. *Coord. Chem. Rev.* **1988**, *84*, 47.

(14) Isci, H.; Mason, R. *Inorg. Chem.* **1985**, *24*, 1761.

(15) Mann, K. R.; Gordon, J. G., II; Gray, H. B. *J. Am. Chem. Soc.* **1975**, *97*, 3553.

(16) (a) King, C.; Auerbach, R. A.; Fronczek, F. R.; Roundhill, D. M. *J. Am. Chem. Soc.* **1986**, *108*, 5626. (b) Roundhill, D. M.; Shen, Z.-P.; King, C.; Atherton, S. J. *J. Phys. Chem.* **1988**, *92*, 4088.

(17) (a) Novozhilova, I. V.; Volkov, A. V.; Coppens, P. *J. Am. Chem. Soc.* **2003**, *125*, 1079. (b) Stoyanov, S. R.; Villegas, J. M.; Rillema, D. P. *J. Phys. Chem. B* **2004**, *108*, 12175.

(18) Brummer, J. G.; Crosby, G. A. *Chem. Phys. Lett.* **1984**, *112*, 15.

(19) Leung, K. H.; Phillips, D. L.; Che, C.-M.; Miskowski, V. M. *J. Raman Spectrosc.* **1999**, *30*, 987.

(20) Che, C.-M.; Butler, L. G.; Gray, H. B.; Crooks, R. M.; Woodrusff, W. H. *J. Am. Chem. Soc.* **1983**, *105*, 5492.

(21) Kim, C. D.; Pillet, S.; Wu, G.; Fullagar, W. K.; Coppens, P. *Acta Crystallogr.* **2002**, *A58*, 133.

(22) Møller, C.; Plesset, M. S. *Phys. Rev.* **1934**, *46*, 618.

(23) (a) Casida, M. E.; Jamorski, C.; Casida, K. C.; Salahub, D. R. *J. Chem. Phys.* **1998**, *108*, 4439. (b) Statmann, R. E.; Scuseria, G. E. *J. Chem. Phys.* **1998**, *109*, 8218. (c) Bauernschmitt, R.; Ahlrichs, R. *Chem. Phys. Lett.* **1996**, *256*, 454. (d) Frank, I. Excited-State Molecular Dynamics. Invited Review, SIMU Newsletter, **2001**, *3*, 63−77.

(24) (a) Halls, M. D.; Schlegel, H. B. *Chem. Mater.* **2001**, *13*, 2632. (b) Novozhilova, I. V.; Volkov, A. V.; Coppens, P. *Inorg. Chem.* **2004**, *43*, 2299. (c) Stoyanov, S. R.; Villegas, J. M.; Rillema, D. P. *Inorg. Chem.* **2003**, *42*, 7852. (d) Stoyanov, S. R.; Villegas, J. M.; Cruz, A. J.; Lockyear, L. L.; Reibenspies, J. H.; Rillema, D. P. *J. Chem. Theory Comput.* **2005**, *1*, 95. (e) Fujita, E.; Muckerman, J. T. *Inorg. Chem.* **2004**, *43*, 7636. (f) Klein, A.; van Slageren, J.; Záli, S. *Inorg. Chem.* **2002**, *41*, 5216.

(25) (a) Pople, J. A.; Gill, P. M. W.; Johnson, B. G. *Chem. Phys. Lett.* **1992**, *199*, 557. (b) Johnson, B. G.; Frisch, M. J. *J. Chem. Phys.* **1994**, *100*, 7429.

(26) (a) Wadt, W. R.; Hay, P. J. *J. Chem. Phys.* **1985**, *82*, 284. (b) Hay, P. J.; Wadt, W. R. *J. Chem. Phys.* **1985**, *82*, 299.

(27) (a) Pyykkö, P.; Runeberg, N.; Mendizabal, F. *Chem.—Eur. J.* **1997**, *3*, 1451. (b) Pyykkö, P.; Mendizabal, F. *Chem.—Eur. J.* **1997**, *3*, 1458. (c) Pyykkö, P.; Mendizabal, F. *Inorg. Chem.* **1998**, *37*, 3018.

(28) (a) Pan, Q.-J.; Zhang, H.-X. *Inorg. Chem.* **2004**, *43*, 593. (b) Pan, Q.-J.; Zhang, H.-X. *J. Phys. Chem. A* **2004**, *108*, 3650. (c) Pan, Q.-J.; Zhang, H.-X. *Organometallics* **2004**, *23*, 5198.

consistent reaction field (SCRF)[29] method to account for the solvent effect of water. Combined with the PCM solvent-effect model, the absorption and emission of such complexes in the aqueous solution were obtained under the TD-DFT calculations. Here, the $C_{2h}$ symmetry was adopted to settle the ground- and excited-state conformations of **pop**, **pcp**, and **pop**'s derivatives. All the calculations were accomplished by using the *Gaussian03* program package.[29]

## Results and Discussion

In the past two decades, extensive studies were carried out on the photophysical and photochemical properties of the binuclear platinum(II) complexes, $Y_n[Pt_2(pop)_4]$ ($Y = K^+$, $(n\text{-}Bu_4N)^+$, $Ba^{2+}$, and $(Et_4N)_3H^{4+}$).[2−10] Their intense phosphorescent emission at ca. 512 nm in water was assigned as a metal-centered (MC) transition by theoretical[17] and experimental[3,4] studies. At room temperature, the triplet excited state, $[Pt_2(pop)_4]^{4-*}$, can perform a variety of energy-, electron-, and atom-transfer reactions.[5−7] The single-crystal X-ray structure of $K_4[Pt_2(pop)_4]\cdot 2H_2O$ showed the anion with an eclipsed "lantern" type structure, which has planar platinum(II) centers linked by an $\mu$-pop group. The anion has a Pt−Pt separation of 2.925 Å with no ligands bonded to the axial sites.[2]

Many investigations on $[Pt_2(pop)_4]^{4-}$ have greatly promoted interest in its related species, such as $[Pt_2(pcp)_4]^{4-}$and $[Pt_2(pop)_4X_2]^{4-}$ (X = I, Br and Cl). The isoelectronic pcp complex also possesses similar structure and spectroscopic properties.[16] However, the halide derivatives display shorter Pt−Pt distances and different featured spectra compared with their parent complex.[11−14] Therefore, an insight into the nature of these complexes in the ground and excited states contributes to specifying their similarities and differences in spectroscopic properties and chemical reactions and extending their existing and potential applications.

**Ground-State Geometries.** In this work, the geometries of **pop**, **pcp**, **popI**, **popBr**, **popCl**, and $\mathbf{pop}^{2+}$ in the ground states were optimized using the MP2 method. Their structures are presented in Figure 1 with the depicted coordinate orientation (the *z* axis goes through the two Pt atoms). Selected results from the geometry optimizations on the complexes are listed in Tables 1 and 2 for comparison with the data from the X-ray crystallographic determination of $K_4[Pt_2(pop)_4]\cdot 2H_2O$[2], $K_4[Pt_2(pcp)_4]\cdot 6H_2O$,[16a] and $K_4[Pt_2(pop)_4X_2]\cdot nH_2O$ (X = I, Br, and Cl).[11ab,12,13]

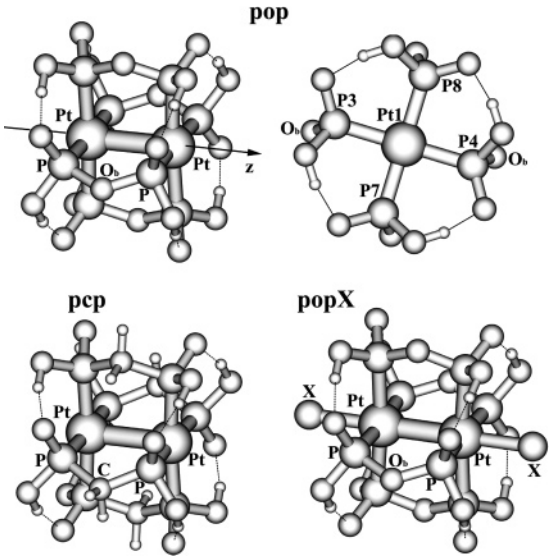


**Figure 1.** Structures of **pop** (right side is a lateral view from the Pt−Pt orientation), **pcp**, and **popX** (X = I, Br, and Cl).

**Table 1.** Optimized Geometry Parameters of $[Pt_2(pop)_4]^{4-}$ (**pop**) and $[Pt_2(pcp)_4]^{4-}$ (**pcp**) Using the MP2 Method for the $^1A_g$ Ground State and the UMP2 Method for the $^3A_u$ Excited State

| | **pop** | | | **pcp** | | |
|---|---|---|---|---|---|---|
| parameters | $^1A_g$ | exp[a] | $^3A_u$ | $^1A_g$ | exp[a] | $^3A_u$ |
| bond length (Å) | | | | | | |
| Pt−Pt | 2.905 | 2.925 | 2.747 | 2.987 | 2.980 | 2.813 |
| Pt−P | 2.373 | 2.320 | 2.389 | 2.368 | 2.328 | 2.384 |
| P−OH | 1.662 | 1.579 | 1.661 | 1.696 | 1.608 | 1.697 |
| P═O | 1.576 | 1.519 | 1.577 | 1.594 | 1.530 | 1.592 |
| P−$O_b$/C | 1.712 | 1.623 | 1.711 | 1.869 | | 1.864 |
| P···P | 3.063 | 2.980 | 3.008 | 3.189 | | 3.132 |
| bond angle (deg) | | | | | | |
| P3−Pt1−P4 | 176.2 | | 173.7 | 175.1 | | 172.3 |
| P3−Pt1−P7 | 89.9 | | 89.8 | 89.9 | 89.9 | 89.7 |
| P3−Pt1−Pt2 | 91.9 | 90.7 | 93.1 | 92.5 | 91.8 | 93.8 |
| P−$O_b$/C−P | 127.0 | 133.3 | 123.0 | 117.2 | 117.1 | 114.3 |

[a] The X-ray crystal diffraction data of $K_4[Pt_2(pop)_4]\cdot 2H_2O$ and $K_4[Pt_2(pcp)_4]\cdot 6H_2O$ from refs 2 and 16a, respectively.

It is shown in Tables 1 and 2 that similarities and differences are found between the calculated and the experimental parameters. For **pop**, the calculated Pt(II)−Pt(II) distance is 2.905 Å, much closer to the distance of 2.925 Å for $K_4[Pt_2(pop)_4]\cdot 2H_2O$[2]. The two Pt(II) atoms tend to approach each other, which is indicated by the 3.063 Å P···P bite distance being more than the Pt−Pt distance, and the 91.9° P−Pt−Pt angle being greater than a right angle. Recently, Coppens[17a] and Rillema[17b] have used DFT methods to optimize the structure of such a complex. Because the DFT method does not precisely describe the metal−metal interaction, the Pt−Pt distance was overestimated by ca. 0.12 Å in their studies. As shown in Table 1, the other geometry parameters slightly deviate from the corresponding experimental values. The largest difference is ca. 0.09 Å for Pt−$O_b$ in distances and ca. 6° for P−$O_b$−P in angles. Each divalent platinum atom exhibits square-planar coordination with four phosphorus atoms from the pyrophosphate ligands, which is reflected in the 176.2° P3−Pt1−P4 and 89.9° P3−Pt1−P7 angles. It is shown in Table 1 that the optimized

(29) Frisch, M. J.; Trucks, G. W.; Schlegel, H. B.; Scuseria, G. E.; Robb, M. A.; Cheeseman, J. R.; Montgomery, J. A., Jr.; Vreven, T.; Kudin, K. N.; Burant, J. C.; Millam, J. M.; Iyengar, S. S.; Tomasi, J.; Barone, V.; Mennucci, B.; Cossi, M.; Scalmani, G.; Rega, N.; Petersson, G. A.; Nakatsuji, H.; Hada, M.; Ehara, M.; Toyota, K.; Fukuda, R.; Hasegawa, J.; Ishida, M.; Nakajima, T.; Honda, Y.; Kitao, O.; Nakai, H.; Klene, M.; Li, X.; Knox, J. E.; Hratchian, H. P.; Cross, J. B.; Bakken, V.; Adamo, C.; Jaramillo, J.; Gomperts, R.; Stratmann, R. E.; Yazyev, O.; Austin, A. J.; Cammi, R.; Pomelli, C.; Ochterski, J. W.; Ayala, P. Y.; Morokuma, K.; Voth, G. A.; Salvador, P.; Dannenberg, J. J.; Zakrzewski, V. G.; Dapprich, S.; Daniels, A. D.; Strain, M. C.; Farkas, O.; Malick, D. K.; Rabuck, A. D.; Raghavachari, K.; Foresman, J. B.; Ortiz, J. V.; Cui, Q.; Baboul, A. G.; Clifford, S.; Cioslowski, J.; Stefanov, B. B.; Liu, G.; Liashenko, A.; Piskorz, P.; Komaromi, I.; Martin, R. L.; Fox, D. J.; Keith, T.; Al-Laham, M. A.; Peng, C. Y.; Nanayakkara, A.; Challacombe, M.; Gill, P. M. W.; Johnson, B.; Chen, W.; Wong, M. W.; Gonzalez, C.; Pople, J. A. *Gaussian 03*, revision C.02; Gaussian, Inc.: Wallingford, CT, 2004.

**Table 2.** Optimized Geometry Parameters of $[Pt_2(pop)_4X_2]^{4-}$ (X = I (**popI**), Br (**popBr**), and Cl (**popCl**)) and $[Pt_2(pop)_4]^{2-}$ (**pop**$^{2+}$) in the $^1A_g$ Ground States Using the MP2 Method

| | **popI** | | **popBr** | | **popCl** | | **pop**$^{2+}$ |
|---|---|---|---|---|---|---|---|
| parameters | $^1A_g$ | exp[a] | $^1A_g$ | exp[a] | $^1A_g$ | exp[a] | $^1A_g$ |
| bond length (Å) | | | | | | | |
| Pt−Pt | 2.802 | 2.754 | 2.775 | 2.723 | 2.758 | 2.695 | 2.666 |
| Pt−P | 2.416 | 2.348 | 2.415 | 2.342 | 2.414 | 2.350 | 2.439 |
| P−OH | 1.652 | 1.565 | 1.652 | 1.529 | 1.651 | 1.557 | 1.640 |
| P═O | 1.570 | 1.504 | 1.571 | 1.529 | 1.571 | 1.512 | 1.557 |
| P−$O_b$ | 1.702 | 1.621 | 1.703 | 1.635 | 1.704 | 1.616 | 1.698 |
| P−X | 2.797 | 2.746 | 2.619 | 2.555 | 2.473 | 2.407 | |
| P···P | 3.008 | | 3.003 | | 2.999 | | 2.941 |
| bond angle (deg) | | | | | | | |
| P3−Pt1−P4 | 175.1 | | 174.6 | 176.0 | 174.3 | | 173.5 |
| P3−Pt1−P7 | 89.8 | 89.9 | 89.9 | | 89.8 | | 89.8 |
| P3−Pt1−Pt2 | 92.5 | 91.8 | 92.7 | 92.0 | 92.9 | 92.2 | 93.2 |
| P−$O_b$−P | 124.2 | 126.9 | 123.7 | 128.8 | 123.3 | 125.5 | 120.0 |

[a] The X-ray crystal diffraction data of $K_4[Pt_2(pop)_4X_2]\cdot nH_2O$ (X = I, Br, and Cl) from refs 11ab, 12, and 13.

geometry parameters of **pcp** agree well with those of $K_4[Pt_2(pcp)_4]\cdot 6H_2O$.[16a] The largest difference in these distances is no more than 0.09 Å. The calculated 2.987 Å Pt−Pt separation is comparable to the experimental distance of 2.980 Å.

With respect to **popX** (X = I, Br, and Cl), the optimized Pt−Pt distances are 2.802, 2.775, and 2.758 Å, respectively (Table 2). The Pt−X bond lengths of 2.797, 2.619, and 2.473 Å correspond to experimental distances of 2.746, 2.555, and 2.407 Å, respectively.[11ab,12,13] Aside from the variations in the Pt−Pt distances, the $[Pt_2(pop)_4]$ skeleton units (Figure 1) are remarkably similar in the **pop** and **popX** complexes. As the Pt−Pt distance shrinks by ca. 0.15 Å in going from **pop** to **popCl**, the P···P distance decreases by only 0.06 Å, the P−$O_b$−P angle decreases by ca. 4°, and the Pt−P bonds lengthen only slightly (Tables 1 and 2). Other variables remain nearly constant.

In the theoretical view, we also optimized the structure of **pop**$^{2+}$. By comparison with those of **pop**, the Pt−Pt separation decreases by ca. 0.24 Å, the P···P distance decreases by ca. 0.12 Å, and the Pt−P bonds lengthen by 0.07 Å (Tables 1 and 2). When compared with other Pt(III)−Pt(III) complexes such as **popX** (X = I, Br, and Cl), **pop**$^{2+}$ has no axial ligands to perturb on the Pt−Pt $\sigma$ bond. So, the Pt−Pt distance of **pop**$^{2+}$ should be the shortest in all the binuclear Pt(III)−Pt(III) complexes as indicated in Table 2.

Formation of a Pt−Pt single bond apparently drives the binuclear oxidative addition reactions from **pop** to **popX**.[11a] Simple MO theory predicted that two Pt−Pt d$\sigma$* electrons are transferred to $X_2$ in each product complex $[(Pt^{II})_2$ is $(d\sigma)^2$-$(d\sigma^*)^2$; $(Pt^{III})_2$ is $(d\sigma)^2]$.[3] The Pt−Pt bonding is weak in the former but much stronger in the latter. In the present studies, we calculated the Pt−Pt distances at 2.905, 2.802, 2.775, 2.758, and 2.666 Å for **pop**, **popX** (X = I, Br, and Cl), and **pop**$^{2+}$, respectively. (Tables 1 and 2) This reproduces well the trend in the Pt−Pt distances determined by experiments.[11,12]

To provide a deep insight into the Pt−Pt bonding, the orbital energy levels of such complexes in the MP2 calculations are presented in Figure 2. We list detailed information of electronic structures in Supporting Information, Tables 1−3. As seen from Figure 2, **pop** has the orbital distribution similar to **pop**$^{2+}$ except that the latter has the empty $\sigma^*(d_{z^2})$ ($28a_u$) orbital and relatively lower-energy orbitals. We roughly calculated that the Pt−Pt bond orders in **pop** and **pop**$^{2+}$ are 0.037 and 0.714, respectively. This can elucidate

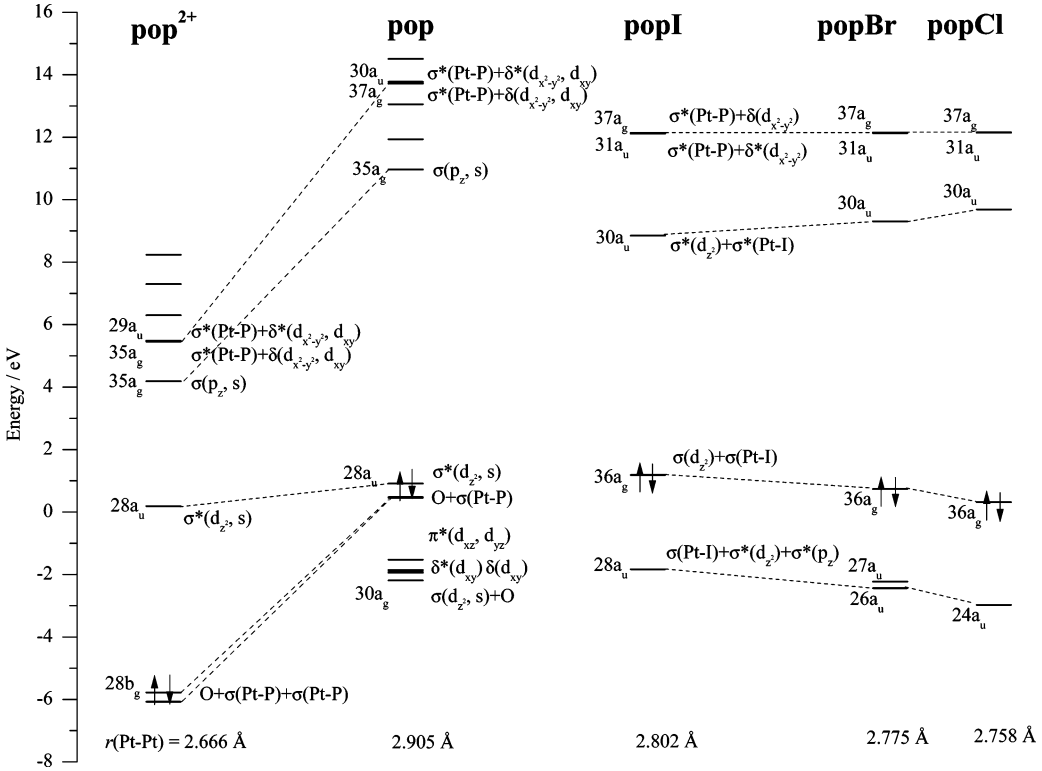


**Figure 2.** Orbital energy levels of **pop**, **popX** (X = I, Br, and Cl), and **pop**$^{2+}$ in the MP2 calculations.

**Table 3.** Calculated Absorptions of **pop** in the Aqueous Solution at the TD-DFT (B3LYP) Level, Associated with the Absorptions Observed in the Experiment

| states | conf | \|CI coef\| > 0.2 | $\lambda$ (nm)[a] | $E$ (eV)[a] | $f$[b] | exp[c] |
|---|---|---|---|---|---|---|
| $^3A_u$ | $28a_u \rightarrow 35a_g$ | 0.738 | 431 | 2.88 | 0.000 | 452 (110) |
| A $^1A_u$ | $28a_u \rightarrow 35a_g$ | 0.665 | 351 | 3.53 | 0.276 | 367 (34500) |
| B $^1B_u$ | $34b_u \rightarrow 35a_g$ | 0.696 | 301 | 4.12 | 0.008 | |
| C $^1B_u$ | $33b_u \rightarrow 35a_g$ | 0.696 | 301 | 4.13 | 0.008 | |
| D $^1B_u$ | $32b_u \rightarrow 35a_g$ | 0.685 | 253 | 4.89 | 0.001 | |
| E $^1B_u$ | $31b_u \rightarrow 35a_g$ | 0.685 | 253 | 4.89 | 0.001 | |
| F $^1B_u$ | $34b_u \rightarrow 36a_g$ | 0.591 | 243 | 5.10 | 0.024 | 266 (1550) |
| | $28b_g \rightarrow 29a_u$ | −0.363 | | | | |
| G $^1B_u$ | $33b_u \rightarrow 36a_g$ | 0.592 | 243 | 5.10 | 0.024 | |
| | $27b_g \rightarrow 29a_u$ | −0.362 | | | | |

[a] Calculated absorption spectra in nm and eV. [b] Oscillator strength. [c] Experimental absorptions from refs 3, 4a, 14, and 30, and molar absorption coefficient ($M^{-1}cm^{-1}$) listed in parentheses.

that the Pt−Pt distance is longer in the former than in the latter. With respect to **popX**, the bonding interactions between the $d_{z^2}$(Pt) and $p_z$(X) orbitals remove a majority of electrons from the filled $\sigma^*(d_{z^2})$ orbitals of **pop**. So, the Pt−Pt bond orders of **popX** should be located between those of **pop** and $\mathbf{pop}^{2+}$. Accordingly, the Pt−Pt distances decrease from **pop** to **popX** to $\mathbf{pop}^{2+}$.

As shown in Figure 2 and Supporting Information, Table 2, **popX** (X = I, Br, and Cl) possess very similiar molecular orbital properties [e.g., highest occupied molecular orbital (HOMOs) of $\sigma(d_{z^2})$ + $\sigma$(Pt−X) and lowest unoccupied molecular orbitals (LUMOs) of $\sigma^*(d_{z^2})$ + $\sigma^*$(Pt−X)]. However, the different $\sigma$-donating strengths of I, Br, and Cl result in the different Pt−Pt distances in **popX**. The calculated results show that the trend in the Pt−Pt distances follows the sequence I > Br > Cl, which can be explained from the detailed analyses on their electronic structures (Supporting Information, Table 2). On one hand, the HOMOs of **popX** (X = I, Br, and Cl) are $\sigma$ bonding characters, which are mainly contributed by 10.8, 14.8, and 19.4% $d_{z^2}$, respectively. More $d_{z^2}$ contribution of Pt atoms favors a stronger Pt−Pt interaction and a shorter Pt−Pt distance. On the other hand, less $p_z$(X) participation in the antibonding LUMOs tends to strengthen the Pt−Pt interaction and shorten the Pt−Pt distance (28.8% $p_z$(I), 21.6% $p_z$(Br), and 16.2% $p_z$(Cl)). Indeed, our calculated bond orders of 0.439, 0.490, and 0.537 for **popX** (X = I, Br, and Cl), respectively, support such a trend in the Pt−Pt distances. In brief, the electronic structures indicate that the Pt−Pt distances vary in the order: **pop** > **popI** > **popBr** > **popCl** > $\mathbf{pop}^{2+}$.

**Absorption Spectra.** TD-DFT based on linear-response theory has recently become a reliable method for prediction of excited-state energies.[24] Here the electronic transition energies of **pop**, **pcp**, and **popX** (X = I, Br, and Cl) were calculated using the TD-DFT (B3LYP) method at their optimized ground-state structures. Combined with the PCM solvent-effect model, we obtained the absorption spectra of such complexes in the aqueous solution. In Tables 3 and 4 and Supporting Information, Tables 4−6, the transition energies (nm/eV) and oscillator strengths of absorptions are listed, which are associated with experimental absorption spectra.[3,4a,11ac,13,16a] We provide detailed information of the MOs involved in absorption transitions in Supporting Information, Tables 7−11.

**Table 4.** Calculated Absorptions of **pcp** in the Aqueous Solution at the TD-DFT (B3LYP) Level, Associated with the Absorptions Observed in the Experiment

| states | conf | \|CI coef\| > 0.2 | $\lambda$ (nm)[a] | $E$ (eV)[a] | $f$[b] | exp[c] |
|---|---|---|---|---|---|---|
| $^3A_u$ | $28a_u \rightarrow 35a_g$ | 0.734 | 452 | 2.74 | 0.000 | 470 (142) |
| A $^1A_u$ | $28a_u \rightarrow 35a_g$ | 0.666 | 369 | 3.36 | 0.214 | 382 (29000) |
| B $^1B_u$ | $34b_u \rightarrow 35a_g$ | 0.696 | 338 | 3.67 | 0.006 | |
| C $^1B_u$ | $33b_u \rightarrow 35a_g$ | 0.696 | 338 | 3.67 | 0.006 | |
| D $^1A_u$ | $27a_u \rightarrow 35a_g$ | 0.701 | 273 | 4.54 | 0.021 | |
| E $^1B_u$ | $28b_g \rightarrow 29a_u$ | 0.690 | 263 | 4.71 | 0.002 | |
| F $^1B_u$ | $27b_g \rightarrow 29a_u$ | 0.690 | 263 | 4.71 | 0.002 | |
| G $^1B_u$ | $28b_g \rightarrow 30a_u$ | 0.658 | 257 | 4.83 | 0.107 | |
| H $^1B_u$ | $27b_g \rightarrow 30a_u$ | 0.658 | 257 | 4.83 | 0.107 | |

[a] Calculated absorption spectra in nm and eV. [b] Oscillator strength. [c] Experimental absorptions from ref 16a, and molar absorption coefficient ($M^{-1}cm^{-1}$) listed in parentheses.

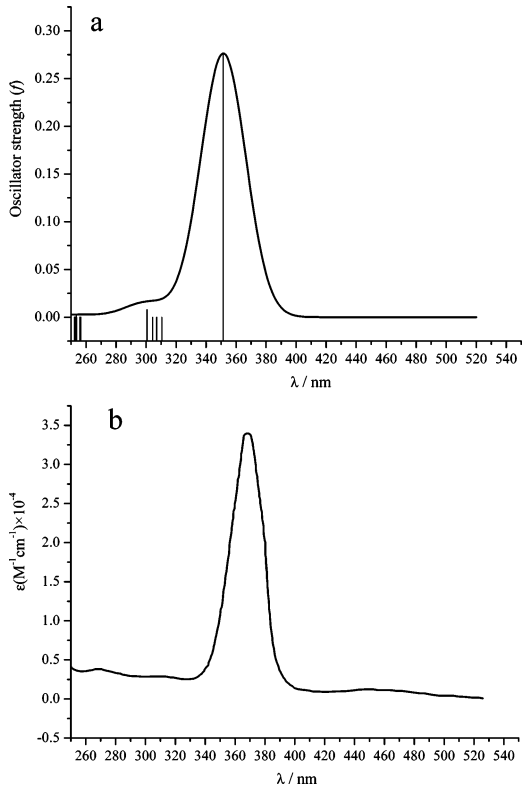


**Figure 3.** Simulated absorption spectra (a) in water for **pop** from the TD-DFT/PCM calculations, together with experimental spectra (b).

In Figure 3a, we have simulated the absorption spectra of **pop** in water on the basis of the TD-DFT/PCM calculations. The theoretical spectrum of **pop** contains an absorption maximum at 351 nm (3.53 eV) and a shoulder at 301 nm (4.12 eV). This is reasonably similar to the experimental spectrum (Figure 3b)[4a] that exhibits absorption maximum at wavelengths of 368 nm with molar absorption coefficient of 34 500 $M^{-1}$ $cm^{-1}$. Our studies reveal the lowest-energy absorption to be dominated by the MC transition (Table 3 and Supporting Information, Table 7). The absorption at 351 nm, which is mainly contributed by the $28a_u \rightarrow 35a_g$ (HOMO → LUMO) configuration, has the largest calculated oscillator strength of 0.276 in the visible region. As shown in

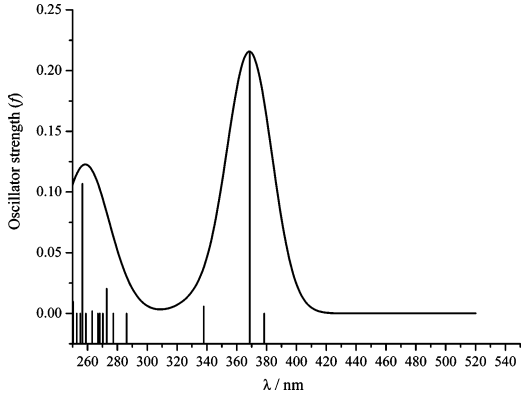


**Figure 4.** Simulated absorption spectra in water for **pcp** from the TD-DFT/PCM calculations.

Supporting Information, Table 7, the absorption is attributed to a $\sigma^*(d_{z^2}) \rightarrow \sigma(p_z)$ transition. It is worth noting that the other absorptions occur in pairs for the **pop** anion should have had the largest point group of $C_{4h}$. The 301 and 253 nm transitions are assigned as $[O + \sigma(Pt-P)] \rightarrow \sigma(p_z)$ and $O \rightarrow \sigma(p_z)$ charge transfers, respectively. The $F^1B_u$ excited state gives rise to absorption at 243 nm, which corresponds to the promotion of an electron into $[\sigma^*(Pt - P) + \delta(d_{x^2-y^2}, d_{xy})]$ and $[\sigma^*(Pt-P) + \delta^*(d_{x^2-y^2}, d_{xy})]$ from $[O_{xz} + \sigma(Pt-P)_x]$. The other three absorptions also have similar transition properties.

Additionally, the triplet excited states related to the dipole-forbidden absorptions also were considered in the TD-DFT calculations on **pop**. As a heavy metal element, the spin−orbit coupling of the Pt atom should be large; thus, the singlet-to-triplet transition may appear as weak tails in the experimental absorption spectra. As shown in Table 3, the lowest-energy absorption from the $X^1A_u \rightarrow {}^3A_u$ transition was calculated at 431 nm (2.88 eV), which belongs to the $\sigma^*(d_{z^2}) \rightarrow \sigma(p_z)$ MC transition. We relate the absorption to the experimental value of 452 nm.[3,4a,14,30]

With respect to **pcp**, the stimulated absorption spectrum (Figure 4) is dominated by two absorption maxima at 369 nm (3.36 eV) and at 257 nm (4.83 eV). The $28a_u \rightarrow 35a_g$ (HOMO → LUMO) transition contributes to the lowest-energy absorption at 369 nm (3.36 eV) with the oscillator strength of 0.214. The dominating absorption corresponds to a $\sigma^*(d_{z^2}) \rightarrow \sigma(p_z)$ MC transition (Supporting Information, Table 8). Similarly, the lowest-energy singlet-to-triplet absorption occurs at 452 nm in the TD-DFT calculations. Experimental studies indicated that the $K_4[Pt_2(pcp)_4]\cdot 6H_2O$ complex exhibits absorption bands at 382 nm ($\epsilon = 29\,000$ $M^{-1}$ $cm^{-1}$) and 470 nm ($\epsilon = 142$ $M^{-1}$ $cm^{-1}$) in the aqueous solution at room temperature.[16a] It is evident that better agreement is found between experimental and calculated absorptions.

Here, according to the calculated absorptions at the TD-DFT/PCM level, we simulated the spectra of **popX** (X = I, Br, and Cl) in Supporting Information, Figures 1−3. For the two featured absorptions observed in experiments,[11ac,13] the intense peak is well reproduced by the theoretical spectra, but the weak peak only corresponds to a shoulder band in the theoretical spectra. For example, the calculated transitions at 317 nm ($f = 0.508$) and 409 nm (0.003) for **popCl** are comparable to the experimental values of 282 nm ($\epsilon =$ 48 840 $M^{-1}$ $cm^{-1}$) and 345 nm (8 190 $M^{-1}$ $cm^{-1}$). The former is assigned as the admixture of $\sigma(d_{z^2}) \rightarrow \sigma^*(d_{z^2})$ and $\sigma(Pt-Cl) \rightarrow \sigma^*(Pt-Cl)$ transitions (Supporting Information, Tables 4 and 9).

Note from Supporting Information, Figures 1−3 and Supporting Information, Tables 4−6 that there are some differences between the calculated and the experimental absorptions. To explore the reason, we used **popCl** as an example to perform the following calculations: (i) B3LYP/PCM at the optimized geometry; (ii) B3LYP/PCM at the experimental geometry; (iii) B3LYP/C-PCM at the optimized geometry; (iv) PBEPBE/PCM (the 1996 functional of Perdew, Burke, and Ernzerhof) at the optimized geometry; and (v) PBEPBE/C−PCM at the optimized geometry. The calculated results are listed in Supporting Information, Table 12. Compared with method (i) used in the present calculations, the results from method (ii) are much closer to the experimental observations and are further supported by the comparison between simulated (the red line in Supporting Information, Figure 1a) and experimental spectra (Supporting Information, Figure 1b).[11c] Therefore, we conclude that the different geometry structures are one of the most important reasons that leads to a large difference between calculated and experimental absorptions.

**Excited-State Properties of pop and pcp.** The studies on the electronic excited state of molecules continue to receive intense attention.[31] So far, the theoretical calculation is one of the most effective means to investigate such problems.[23,24] In this work, the UMP2 methods were used to optimize structures of **pop** and **pcp** in the lowest-energy triple excited states. The geometry parameters are listed in Table 1.

The UMP2 calculations on **pop** predict that the Pt−Pt distance shrinks by ca. 0.16 Å in going from the ground state to the lowest-energy triple excited state, the P···P distance decreases by ca. 0.06 Å, and the Pt−P bonds lengthen ca. 0.02 Å (Table 1). Because the shrinkage of Pt−Pt is much more than that of P···P, the bonding interaction between the two Pt atoms drives the Pt−Pt shrinkage. Over the last two decades, the Pt−Pt distance in the triplet excited state has been studied in many experiments of $Y_n[Pt_2(pop)_4]$ ($Y = K^+$, $(n\text{-}Bu_4N)^+$, $Ba^{2+}$, and $(Et_4N)_3H^{4+}$). Through Frank−Cotton analysis,[3,4b,18] resonance Raman spectra,[19,20] and time-resolved X-ray diffraction,[21] the authors summarized that the Pt−Pt distances in the triplet excited-state range were from ca. 2.64 to 2.71 Å with ca. 0.29−0.21 Å contraction relative

(30) Stiegman, A. E.; Rice, S. F.; Gray, H. B.; Miskowski, V. M. *Inorg. Chem.* **1987**, *26*, 1112.

(31) (a) Nordwig, B. L.; Ohlsen, D. J.; Beyer, K. D.; Wruck, A. S.; Brummer, J. G. *Inorg. Chem.* **2006**, *45*, 858. (b) Dreuw, A.; Head-Gordon, M. *Chem. Rev.* **2005**, *105*, 4009. (c) Bojan, V. R.; Fernandez, E. J.; Laguna, A.; Lopez-de-Luzuriaga, J. M.; Monge, M.; Olmos, M. E.; Silvestru, C. *J. Am. Chem. Soc.* **2005**, *127*, 11564. (d) Sotoyama, W.; Satoh, T.; Sato, H.; Matsuura, A.; Sawatari, N. *J. Phys. Chem. A.* **2005**, *109*, 9760. (e) Kobayashi, A.; Kojima, T.; Ikeda, R.; Kitagawa, H. *Inorg. Chem.* **2006**, *45*, 322.

to 2.91−2.92 Å in the ground state. Results of recent theoretical studies using the DFT method have found excited- and ground-state distances of 2.82 and 3.04 Å, respectively.[17] In the present studies, our MP2 calculations predict the distances at 2.747 and 2.905 Å, respectively (Table 1). Apparently, our calculations agree with such experimental results.

Just like the case in **pop**, optimizations on **pcp** at the UMP2 level show that the Pt−Pt distance decreases by ca. 0.17 Å upon excitation, the P···P distance decreases by ca. 0.06 Å, and the Pt−P bonds lengthen ca. 0.02 Å (Table 1). The bonding interactions between the two Pt atoms in the excited states weaken the P → Pt dative bonds, which leads to the elongation of the Pt−P bond length. Although **pop** and **pcp** have the structural difference in the ligand bridge, their similar changes between the ground and the excited states in the structures imply that the excited electronic transitions mainly occur within the metal centers.

On the basis of such optimized structures, we used the TD-DFT method to calculate the emission energies of **pop** and **pcp**. By including the PCM model in the TD-DFT calculations, we obtained the emissions in the aqueous solution. The calculated emissions in the gas phase and solution are listed in Supporting Information, Table 13 along with the experimental values.[4,16]

In the calculations, TD-DFT predicts the phosphorescent emission energies of **pop** at 2.60 eV (478 nm) in the gas phase and 2.58 eV (480 nm) in water. The solution emission is closer to the experimental value of 2.40 eV (512 nm).[4] According to the analyses on the wave functions of these excited states, we attribute the emissions to the MC $\sigma(p_z) \rightarrow \sigma^*(d_{z^2})$ transitions, which agree with experimental studies.[4] As shown in Supporting Information, Table 13, note that there is a slight difference of emission energies between in the gas phase and in solution. This suggests that interactions between anion and solvent molecules slightly affect the emission spectra. A similar case is found in the calculations on **pcp** (Supporting Information, Table 13). On the basis of the optimized excited-state structure, TD-DFT calculates emission energy at 2.50 eV (496 nm) in the aqueous solution, comparable to 2.43 eV (510 nm) phosphorescence of $K_4[Pt_2(pcp)_4]\cdot 6H_2O$.[16]

## Conclusions

Optimizations on **pop**, **pcp**, **popX** (X = I, Br, and Cl), and $\mathbf{pop}^{2+}$ in the ground states were performed using the MP2 method. Their Pt−Pt distances decrease in going from **pop** to **popX** (X = I, Br, and Cl) to $\mathbf{pop}^{2+}$. This is evidenced by the analyses of their electronic structures.

On the basis of such ground-state structures, TD-DFT with the PCM solvent-effect model was employed to predict the aqueous absorption spectra of **pop**, **pcp**, and **popX** (X = I, Br, and Cl). The calculated results agree with experimental observations. It is found that the $^{1,3}[\sigma^*(d_{z^2}) \rightarrow \sigma(p_z)]$ absorptions in **pop** and **pcp** have the lowest transition energies, and $^1[\sigma^*(d_{z^2}) \rightarrow \sigma(p_z)]$ absorptions possess the largest oscillator strength in the low-lying dipole-allowed transitions (Tables 3 and 4). The dominated absorption bands of such complexes observed by experiments are well reproduced by the simulated theoretical spectra.

The structures of **pop** and **pcp** in the lowest-energy triplet excited states were optimized at the UMP2 level. The Pt−Pt contraction trend is well reproduced in these calculations. UMP2 calculations on **pop** predict the Pt−Pt distance in the excited state at 2.747 Å, which is comparable to experimental values of 2.64−2.71 Å.[3,4b,18−21] Additionally, TD-DFT estimates the solution phosphorescent emissions of **pop** and **pcp** at 480 and 496 nm, respectively, both attributable to the metal-centered $\sigma(p_z) \rightarrow \sigma^*(d_{z^2})$ transitions. The calculated emissions are in accordance with the 512 and 510 nm emissions in experiment, respectively.[4,16]

**Acknowledgment.** This work is supported by the National Natural Science Foundation of China (No. 20301006, 20173021).

**Supporting Information Available:** Tables of MO compositions of **pop**, **popX** (X = I, Br, and Cl), and $\mathbf{pop}^{2+}$ under the MP2 calculations; tables of absorptions of **popX** (X = I, Br, and Cl); tables of MO compositions of **pop**, **pcp** and **popX** (X = I, Br, and Cl) under the TD-DFT calculations; table of calculated absorptions of **popCl** at different structures, density functionals and solvent-effect models; table of calculated emissions of **pop** and **pcp** in the gas phase and aqueous solution; figures of simulated absorption spectra for **popX** (X = I, Br, and Cl). This material is available free of charge via the Internet at http://pubs.acs.org.

IC060336V